Applied and Computational Mechanics 19 (2025) XXX–YYY

Numerical study on the influence of material heterogeneity on mode III crack propagation using a phase-field model

S. Alfat [a,*], R. Eso[a], L. O. A. Barata[b], M. S. Rianse[c]

[a] *Physics Education Department, Halu Oleo University, H.E.A. Mokodompit, Kendari, Southeast Sulawesi, 9323, Indonesia*
[b] *Mechanical Engineering Department, Halu Oleo University, H.E.A. Mokodompit, Kendari, Southeast Sulawesi, 9323, Indonesia*
[c] *Mining Engineering Department, Halu Oleo University, H.E.A. Mokodompit, Kendari, Southeast Sulawesi, 9323, Indonesia*

Received 11 September 2024; accepted 28 May 2025

Abstract

Understanding crack propagation in heterogeneous materials is crucial for predicting the reliability and durability of structural components. In this study, we investigate the influence of material heterogeneity on mode III crack growth using a phase-field model. The phase-field method offers a powerful computational framework for simulating crack initiation, propagation, and branching without explicitly tracking the crack surface. By incorporating material heterogeneity into the phase-field model, we aim to analyze how variations in material properties affect the material's strength and crack path behavior. The numerical simulations will explore complex interactions between cracks and microstructural features, providing insights into how heterogeneity influences fracture mechanics at different length scales. Through this research, we seek to enhance the understanding of crack growth in realistic materials and contribute to developing strategies for optimizing the performance and reliability of engineering structures subjected to mechanical loading. In this study, we utilize the Weibull distribution function to generate heterogeneous materials and calculate the crack propagation problem using the adaptive finite element method. The adaptive mesh method provides precise results and can significantly reduce computation time.

Keywords: heterogeneous materials, mode III crack propagation, phase-field model, Weibull distribution, adaptive finite element method

1. Introduction

The study of crack propagation is a significant issue and a serious problem in the material industry, construction, geophysics, mining, environmental sciences, oil and gas sectors. Particularly in geophysics, mining, and oil and gas industries, investigating crack propagation in heterogeneous materials is a major concern for scientists and engineers. Given that the structure of natural materials is inherently heterogeneous [41], it becomes crucial to study this phenomenon, starting with how material properties are randomly distributed and observing the behavior of cracks in the material. Some studies on this phenomenon were initiated three decades ago. Several well-established models have been used to study crack propagation, including the discreet element method (DEM) [14, 26], peridynamics [1, 33], damage models [16, 35], and phase-field models [6, 32, 40, 45]. Meanwhile, among these mentioned models, two methods to generate random material properties were introduced, such as the Gaussian random field and the Weibull distribution function. Among these models and methods, the phase-field model and the Weibull distribution function have attracted significant attention from researchers.

*Corresponding author. Tel.: +62 852 418 769 94, e-mail: sayahdin.alfat@yahoo.com.
https://doi.org/10.24132/acm.2025.929

One powerful type of crack propagation model is the phase-field model for crack propagation. This model offers several advantages, including its ability to easily detect crack paths and extensions in 2D and 3D domains, its simplicity in modeling crack propagation without requiring complex algorithms, and its capability to be readily extended to probe cracks in multi-physics problems [3, 12, 23, 31]. Originally, the model was introduced by Bourdin et al. [13] and Karma et al. [22] for brittle crack propagation. Then, the model has been extended to many applications, such as ductile crack propagation [9], crack propagation in viscoelasticity [4, 22, 23], crack propagation in rock-like materials [40, 45], crack propagation in anti-plane displacement [3, 23, 37], crack propagation due to thermal effects [5, 7, 23, 31], fluid pressure [2, 3, 21, 32], desiccation cracking [21, 30], and hydrogen embrittlement [15, 23, 31]. While several studies have demonstrated crack extension in heterogeneous materials using the Weibull distribution function [32, 40, 43], most of them have treated mode I or mode I and II fractures and not much regarding mode III behavior. Moreover, while the Weibull distribution has been utilized to introduce randomness in material characteristics, its specific application to prepare spatially inhomogeneous materials for mode III crack extension tasks is not much discussed. In addition, the concept of a homogeneity index—as a scalar value derived from the Weibull distribution parameters to quantify material randomness—has not been covered by a systematic investigation. This study aims to fill these gaps by (i) generating heterogeneous materials through the Weibull distribution function, (ii) introducing a homogeneity index to quantify levels of randomness, and (iii) examining their effects on mode III crack propagation through a phase-field method.

Based on the aforementioned statements, the objective of this study is to investigate how variations in material properties affect the strength and crack path behavior of materials. Our specific focus is on the behavior of mode III crack propagation in heterogeneous materials generated by the Weibull distribution function, which we believe has not been explored to date. Additionally, we calculate the phase-field model for crack propagation using FreeFEM++ [20]. This software is an open-source platform focused on solving partial differential equations using the finite element method. The software offers convenience during the calculation of the phase-field model for crack propagation, particularly using adaptive remeshing techniques [7, 17, 23].

The present paper is organized into four sections. The mathematical formulation is presented in Section 2, which is divided into three subsections. The first subsection introduces the governing equation for modeling crack propagation and explains how to derive the crack propagation equation. The second subsection discusses the generation of heterogeneous materials using the Weibull distribution function. The third subsection details the computational setup for the present study. In Section 3, the results and discussion related to the present study are presented. The final section summarizes the findings and outlines future work for the study.

2. Mathematical formulation

2.1. Phase-field model for crack propagation

In the present study, we apply the phase-field model (PFM) for scalar anti-plane crack propagation (mode III crack propagation) in linear elasticity as proposed by Takaishi and Kimura [37]. Since we neglect the friction coefficient and density in the force balance equation, the model is written as follows

$$\begin{aligned} -\text{div}\left[(1-z)^2\mu\nabla u\right] &= 0 && \text{in } \Omega, \\ \alpha\frac{\partial z}{\partial t} &= \left(\varepsilon\ \text{div}\left(\gamma\nabla z\right) - \frac{\gamma}{\varepsilon}z + \mu|\nabla u|^2(1-z)\right)_+ && \text{in } \Omega, \end{aligned} \tag{1}$$

where $u(x,t) = [0, 0, u_3(x_1, x_2)]^T$ is the scalar anti-plane displacement. The variable $z(x,t) \in (0,1)$ is the damage variable, where $z = 0$ represents the uncracked area and $z = 1$ represents the cracked area. The variables $\mu > 0$ and $\gamma > 0$ are the Lame's constant and the critical energy release rate, respectively. The parameters $\alpha > 0$ and $\varepsilon > 0$ represent small regularization parameters for time and length, respectively. Furthermore, α can be referred to as the velocity-dependent fracture energy [24]. In addition, "div" and ∇ denote the divergence and gradient operators, respectively. Equation $(1)_1$ represents the force balance equation governing crack propagation. Here, we neglect the external force $f(x)$ for simplicity.

Equation $(1)_2$ corresponds to the damage evolution equation, where the driving force for crack propagation is given by the term $\mu|\nabla u|^2$. Since crack propagation is an irreversible process, the damage evolution equation $(1)_2$ includes the operator $(\cdot)_+$, defined as $(a)_+ = \max(a, 0)$, to ensure irreversibility.

Equation (1) is completed by the following boundary conditions:

$$u = g(x,t) \text{ on } \Gamma_D^u, \qquad \frac{\partial u}{\partial n} = 0 \text{ on } \Gamma_N^u, \qquad \frac{\partial z}{\partial n} = 0 \text{ on } \Gamma, \tag{2}$$

where n is the outward unit normal vector on the boundary $\partial\Omega = \Gamma = \Gamma_D^u \cup \Gamma_N^u$. Γ_D^u and Γ_N^u represent the Dirichlet and Neumann boundary conditions for displacement, respectively. Equation (1) is supported by the following initial condition:

$$z\big|_{t=0} = z_*(x) \text{ in } \Omega, \qquad u\big|_{t=0} = u_*(x) \text{ in } \Omega \tag{3}$$

with z_* and u_* as the initial crack and displacement, respectively.

The phase-field model for crack propagation, as shown in (1), is derived as a unidirectional gradient flow of elastic $E_{\text{el}}(u,z)$ and surface $E_s(z)$ energies

$$E_{\text{el}}(u,z) = \frac{1}{2}\int_\Omega (1-z)^2 \mu |\nabla u|^2 \, \mathrm{d}x, \tag{4}$$

$$E_s(z) = \frac{1}{2}\int_\Omega \left[\gamma\left(\varepsilon|\nabla z|^2 + \frac{1}{\varepsilon}|z|^2\right)\right] \mathrm{d}x. \tag{5}$$

Equations (4)–(5) are usually called Ambrosio-Tortorelli regularization [10]. In this study, we do not present the derivation of (1) via gradient flow; readers can be referred to [23] for further details. Alternatively, given the similarity between the damage evolution equation and the Ginzburg-Landau equation, we can derive (1) using the microforce balance method (based on the Gurtin's concept) [19]. We will provide this derivation subsequently.

2.2. Derivation of PFM for fracture

Let us consider the Helmholtz free energy Ψ^* and the (pseudo)energy dissipation Φ^* within the phase-field model (PFM) for scalar anti-plane crack propagation

$$\Psi^* = \frac{1}{2}\mu_z |\nabla z|^2 + \frac{1}{2}\gamma\left(\varepsilon|\nabla z|^2 + \frac{1}{\varepsilon}|z|^2\right), \tag{6}$$

$$\Phi^* = \frac{1}{2}D^* = \frac{1}{2}\alpha|\dot{z}|^2, \tag{7}$$

where $\mu_z = (1-z)^2\mu$. Equation (6) can also be referred to as the sum of the elastic and surface energy densities. Equation (7) is obtained using the energy dissipation identity, as clearly

demonstrated in Theorem 2.3 of [5]. Alternatively, it can be obtained by the Clausius-Duhem inequality, as shown in Appendix.

Following the established formalism, we derive the stress function and two internal microscopic force functions as follows

$$P^* = \mu_z \nabla u = \frac{\partial \Psi^*}{\partial \nabla u} + \frac{\partial \Phi^*}{\partial \nabla \dot{u}} = (1-z)^2 \mu \nabla u, \tag{8}$$

$$B^* = \frac{\partial \Psi^*}{\partial z} + \frac{\partial \Phi^*}{\partial \dot{z}} = -(1-z)\mu |\nabla u|^2 + \frac{\gamma z}{\varepsilon} + \alpha \dot{z}, \tag{9}$$

$$H^* = \frac{\partial \Psi^*}{\partial \nabla z} + \frac{\partial \Phi^*}{\partial \nabla \dot{z}} = \gamma \varepsilon \nabla z. \tag{10}$$

From (8), the force balance equation for crack propagation under anti-plane displacement follows from the principle of momentum balance [5]

$$\begin{aligned} \varrho \frac{\partial^2 u}{\partial t^2} &= \text{div}(P^*) + f(x,t) = \text{div}\left[(1-z)^2 \mu \nabla u\right] + f(x,t), \\ \varrho \frac{\partial^2 u}{\partial t^2} &- \text{div}\left[(1-z)^2 \mu \nabla u\right] = f(x,t). \end{aligned} \tag{11}$$

Under quasi-static conditions and in the absence of external forces, equation (11) simplifies to

$$-\text{div}\left[(1-z)^2 \mu \nabla u\right] = 0,$$

which matches equation $(1)_1$, representing the static equilibrium condition of the system.

Meanwhile, the damage evolution equation is derived by substituting (9)–(10) into the microforce balance equation [5, 11, 25], with the micro inertia effect being neglected,

$$\begin{aligned} B^* - \text{div}\, H^* &= 0, \\ \alpha \dot{z} &= \text{div}\, H^* - \frac{\gamma}{\varepsilon} z + (1-z)^2 \mu |\nabla u|^2, \\ \alpha \dot{z} &= \left(\varepsilon\, \text{div}\,(\gamma \nabla z) - \frac{\gamma}{\varepsilon} z + (1-z)^2 \mu |\nabla u|^2\right)_+. \end{aligned} \tag{12}$$

Finally, we have fully derived (1) using the microforce balance model. Based on this method, we ensure that the phase-field model for scalar anti-plane displacement crack propagation in (1) is obviously thermodynamically consistent.

2.3. Weibull function distribution

In the present study, we investigate mode III crack propagation in a heterogeneous material. Therefore, we address the generation of heterogeneous materials in this section. Generally, there are two popular methods to generate heterogeneous materials in probability distribution theory and statistics. The first method uses a Gaussian random field [34, 36], and the second method involves using the Weibull distribution function [28,32,40,41]. In this study, we choose the Weibull distribution function to generate heterogeneous materials.

Let us consider the probability density function of the Weibull distribution

$$f(x_r) = \frac{m}{x_0} \left(\frac{x_r}{x_0}\right)^{m-1} \exp\left[-\left(\frac{x_r}{x_0}\right)^m\right], \tag{13}$$

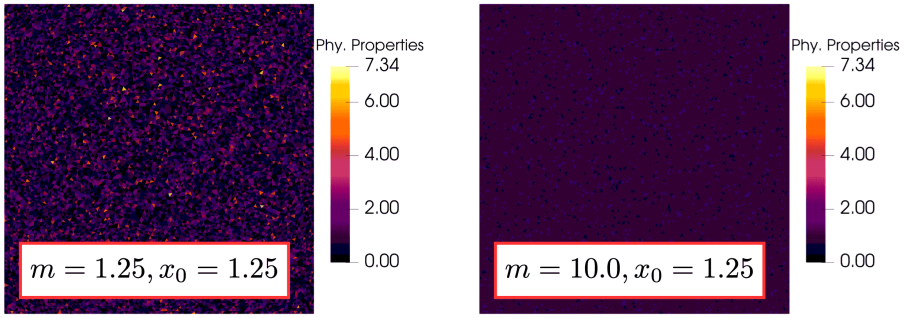

Fig. 1. Parameter x_r distribution profiles for different homogeneity indices m in a 2D domain

where $x_r > 0$ denotes the random physical property parameter of the material element at the mesoscale, $x_0 > 0$ represents the statistical average of these physical property parameters. The parameter $m > 0$ is referred to as the homogeneity index of the material. Originally, equation (13) is the derivative of the cumulative distribution function (CDF) of the Weibull distribution given in (14) with respect to x_r

$$F(x_r) = 1 - \exp\left[-\left(\frac{x_r}{x_0}\right)^m\right]. \tag{14}$$

As a remark, if the parameter m is higher, it indicates that the physical parameter of the material tends to be more homogeneous, and its value approaches x_0. To clarify the influence of different m values on the parameter homogenization index, refer to Figs. 1 and 2.

Since we are dealing with heterogeneous materials, we randomly distribute the physical parameters μ and γ. Therefore, for convenience, we define them as $\mu = \mu_0 x_r$ and $\gamma = \gamma_0 x_r$ to incorporate random distribution, where $\mu_0 = E_y/[2(1+\nu_p)]$ and γ_0 are positive parameters related to the Lame's constant and the energy release rate parameter, respectively. We do not configure the physical properties of heterogeneously distributed materials as done in [27, 39]. Nevertheless, this is also an interesting topic for future work as an extension of this study.

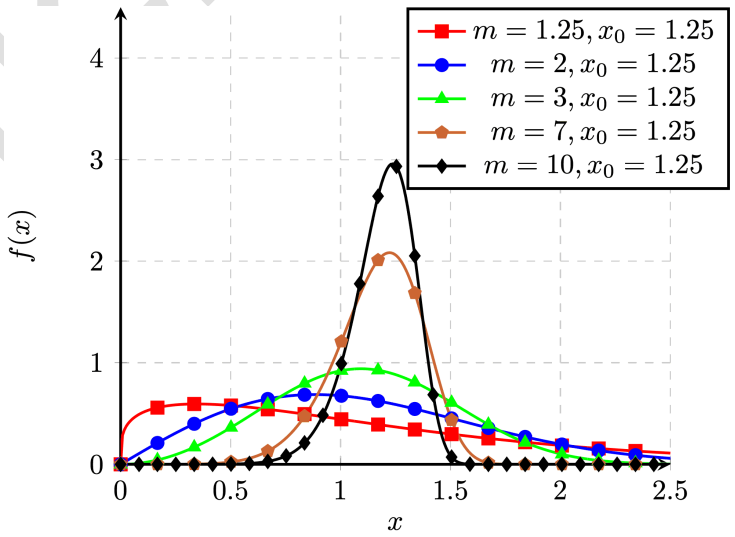

Fig. 2. Profile of $f(x_r)$ for different m

2.4. Computational setup

Herein, we explain the details of the computational setting. Firstly, we start by constructing the time discretization for (1). Let us consider a constant time increment $\Delta t > 0$ and denote the approximate solutions of u and z at time $t = k\Delta t$ ($k = 1, 2, \ldots$) by u^k and z^k, respectively. Considering this and the semi-implicit time discretization scheme [6,37], we have the following time discretization scheme:

$$\begin{aligned} 0 &= \text{div}\left[\left(1 - z^{(k-1)}\right)^2 \mu \nabla u^k\right], \\ \alpha \frac{\tilde{z}^k - z^{(k-1)}}{\Delta t} &= \varepsilon\, \text{div}\left(\gamma \nabla \tilde{z}^k\right) - \frac{\gamma}{\varepsilon}\tilde{z}^k + \mu \left|\nabla u^{(k-1)}\right|^2 \left(1 - \tilde{z}^k\right), \\ z^k &= \max\left(\tilde{z}^k, z^{(k-1)}\right), \end{aligned} \tag{15}$$

where $(15)_3$ represents the irreversible condition $(\cdot)_+$ in equation $(1)_2$.

Equations (15) are calculated using the adaptive finite element method. This is a variant of the finite element method that involves remeshing the triangles at each time step. Herein, we remesh the triangles at each time step based on the damage variable z. The detailed algorithm for the adaptive finite element method is shown in Algorithm 1. The code is written in FreeFEM [20] and run on a MacBook Pro with an Apple M2 chip and 24GB of memory. Meanwhile, ParaView is used as the visualization tool. As a remark, since the small regularization parameter for length ε should be chosen as small as possible, the mesh size h_{min} must be set smaller than ε or $h_{\text{min}} \leq \varepsilon/4$ [12]. Consequently, the computational time becomes significant. Therefore, this is our strong reason for choosing the adaptive finite element method in the computational calculation step, as it can significantly decrease the computational time [4, 17].

The finite element scheme does employ quadratic elements so accuracy is higher, especially when steep gradients are captured near the crack tip that is necessary in fracture phase-field modeling. The resulting linear systems are solved via the LU decomposition method. This method provides a direct factorization of the system matrix into lower and upper triangular matrices, enabling an exact solution in a finite number of steps. It is numerically stable and efficient for problems of moderate size, where computational resources are sufficient to handle the full matrix storage and operations without excessive cost.

Algorithm 1. Adaptive meshing for phase field fracture simulations

Set: $\mathcal{T}_h^0$ an initial mesh;
Set: Initial conditions for z;
Loop
for $k = 1, \cdots, T/\tau$; **do**
  Set $\mathcal{T}_h^k = \mathcal{T}_h^{k-1}$;
  Compute solution of (u^k, z^k) from (15) on mesh $\mathcal{T}_h^k$;
  Set indicator $v \leftarrow$ based on z^k;
  Refine mesh:
  Construct $\mathcal{T}_h^k \leftarrow$ adaptmesh($\mathcal{T}_h^k$, v, $hmin = 1e-5$, $hmax = 0.025$, $nbvx = 1e7$);
  if Refinement is sufficient; **then**
    Break;
  end if
end for

Table 1. List of non-dimensional parameters

Physical properties	μ_0	γ_0	α	ε	x_0	Δt	k
Value	19.4[a]	0.50	1.0	0.01[b]	1.25[c]	0.1	500.0

[a] We obtain it from the Young's modulus E_y and the Poisson ratio ν_p by $\mu_0 = \frac{E_y}{2(1+\nu_p)}$.

[b] Since we choose $\varepsilon = 0.01$, h_{min} is set to 1×10^{-5}.

[c] The parameter is set for Example I, while x_0 is set to 1 for Example II.

The present study uses non-dimensional parameters for simplicity. Therefore, equation (15) should be transformed into non-dimensional form. Herein, we do not detail the transformation process. However, readers can find this information in [5]. For convenience, we list the physical and computational parameters in Table 1.

We investigate crack propagation due to tearing mode (mode III) in the 2D square domain $\Omega = (-1,-1) \times (1,1)$. Herein, the domain includes the horizontal initial crack $z_* = \zeta_0(x_1 + 0.2, x_2)$, where the function ζ_0 is clearly defined in [23]. Additionally, the domain is loaded by displacement $u = \pm gt$ on $\Gamma^u_{\pm D}$ with $\Gamma^u_{\pm D} = \Gamma \cap \{x_2 = \pm 1\}$. For a detailed illustration of the domain, see Fig. 3.

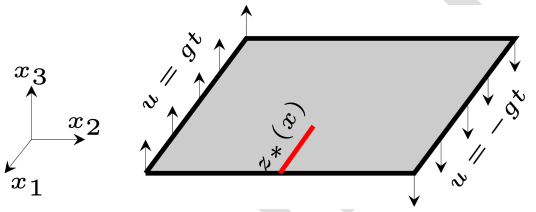

Fig. 3. The domain illustration including the initial crack. The red line represents the initial crack $z_*(x)$, and the given displacement is set to $g = 0.01$

3. Results and discussion

3.1. Results

We considered two experiments to observe the effect of material heterogeneity on the strength and crack path behavior of materials in the present study.

3.1.1. Example I: Effect of homogeneity index m

We vary the homogeneity index m as 1.25, 2.0, 3.0, 7.0, 10.0, and 40.0, with the number of material elements set to 54 668 in this example. The influence of the homogeneity index significantly affects the crack pattern and material strength, as depicted in Figs. 4 and 5a. From Fig. 4, it is evident that the crack path exhibits kinking, deflecting, and branching in materials with m values of 1.25, 2.0, 3.0, and 7.0. In materials with $m = 10.0$, only a kinked crack path is observed, while a straight crack path emerges in materials with $m = 40$. Additionally, another interesting observation in Fig. 4 is that the greater the value of m, the larger the crack area. This is seen from the widening red gradient around the crack area. This is also confirmed in Fig. 5b, which shows that larger crack surface areas occur in materials with large m values. The thickening or expansion of the crack area in the material with $m = 40$ can be understood because the critical energy release rate γ is very small in all areas of the material, causing the

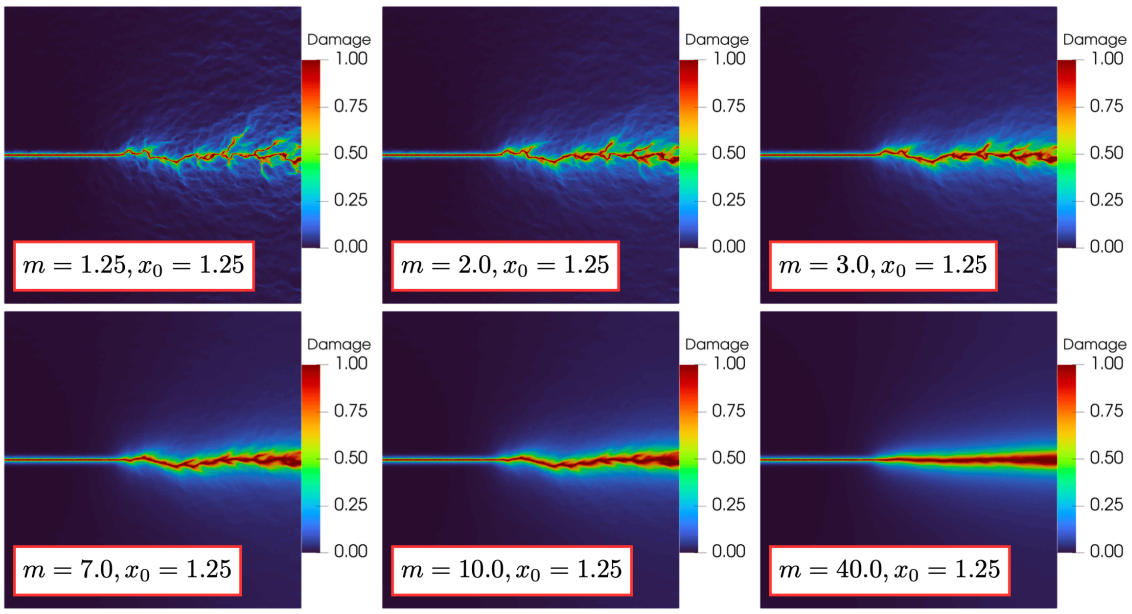

Fig. 4. Crack propagation profiles for different m at final time $t = 50$

crack to diffuse quickly. As a remark, in Fig. 4, the red and blue colors represent cracked and uncracked areas, respectively.

In Fig. 5a, it is evident that the homogeneity index m significantly impacts material strength. A material with a smaller m tends to break or crack easily, whereas a larger m tends to be sturdier. This can be observed through the elastic energy maxima for each m. The highest elastic energy maxima correspond to $m = 40.0$, 10.0, 7.0, 3.0, 2.0, and 1.25, respectively, indicating that higher m values result in stronger materials.

3.1.2. Example II: Heterogeneous influence on a material having interfaces

In this example, we consider the heterogeneous random physical properties with $x_0 = 1$ and $m = 4.0$ of the interface material and investigate their effect on crack propagation behavior. The number of random material elements is similar to Example I. Here, we consider two cases: In the first case, the interface spacing is set to $\delta = 0.2$, while the angle of the interface direction

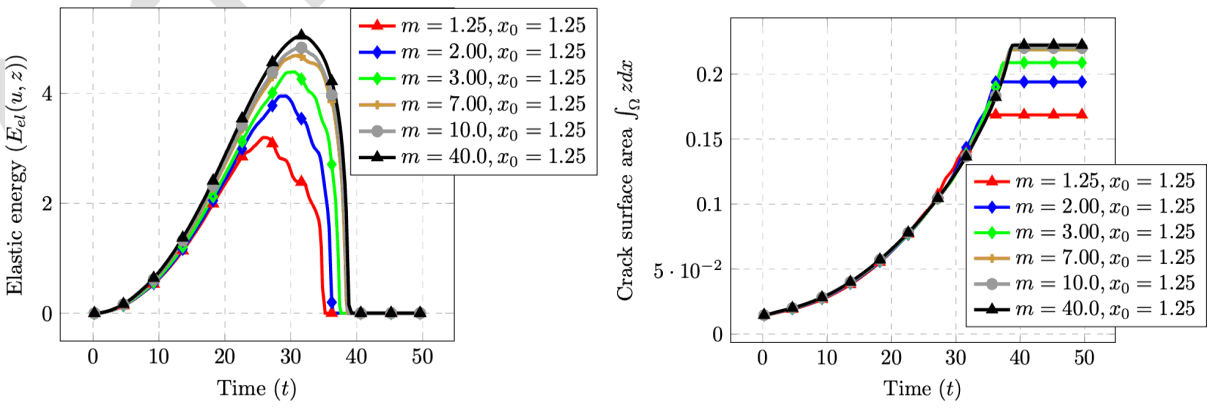

(a) (b)

Fig. 5. (a) Elastic energy and (b) crack surface area profiles for different m during crack propagation

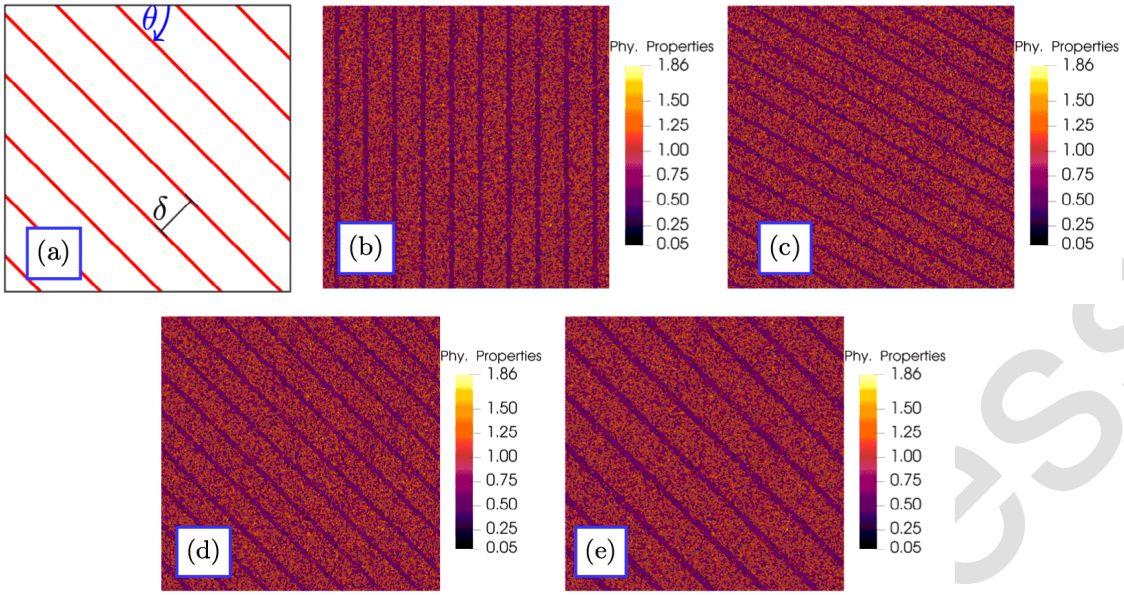

Fig. 6. (a) The domain illustration for Example II: Illustration of profile distribution of x_r in a two-dimensional domain that has diagonal interfaces (the dark area), (b)–(c) represent the first case, and (d)–(e) represent the second case

θ is varied as $\pi/2$, $\pi/3$, $\pi/4$, and $\pi/6$; in the second case, the interface angle is set to $\theta = \pi/4$, while the interface spacing δ is varied as 0.2, 0.275, 0.325, and 0.375. For simplicity, we provide the illustration in Fig. 6. It is important to note that the interface area is designated as the weakest area in the domain, and the physical properties in the interface area are set randomly. We consider the interface region the weakest area because it typically has very low bonding strength. This region is also often referred to as the crack zone. To see the influence of heterogeneous properties on the interface material, we compare the results of each variation of width δ and angle θ on a heterogeneous material with those on a homogeneous material.

Fig. 7 shows the crack profile for different interface directions θ in heterogeneous and homogeneous materials. Herein, it is shown that the influence of heterogeneity in the interface material is very significant in changing the crack path, except in the material with an interface angle of $\pi/6$, see Fig. 7a. At the interface angles $\pi/2$, $\pi/3$, and $\pi/4$, the cracks in the domain do not grow along the interface cracks. However, if the $\pi/6$ angle is used, the crack in the domain is deflected and then grows along the interface, behaving the same as cracks in homogeneous materials. This indicates that the heterogeneity effect has no impact on materials with interface angles less than or equal to $\pi/6$.

For the second case, the result is shown in Fig. 8. It shows that heterogeneity effects only occur at interface materials with $\delta = 0.2$ and 0.275. This is evidenced by the crack profiles, which are clearly different from those in homogeneous materials. Meanwhile, the heterogeneity effect does not apply to interface materials with $\delta = 0.325$ and 0.375; both crack profiles are the same as those of homogeneous materials, which are deflected and then grow along the interface.

3.2. Discussion

In the present study, we investigated crack propagation due to mode III in random heterogeneous materials. The differences in crack behavior observed in Example I were attributed to variations in the m values. If we use a small value of m, the minimum value of the random physical

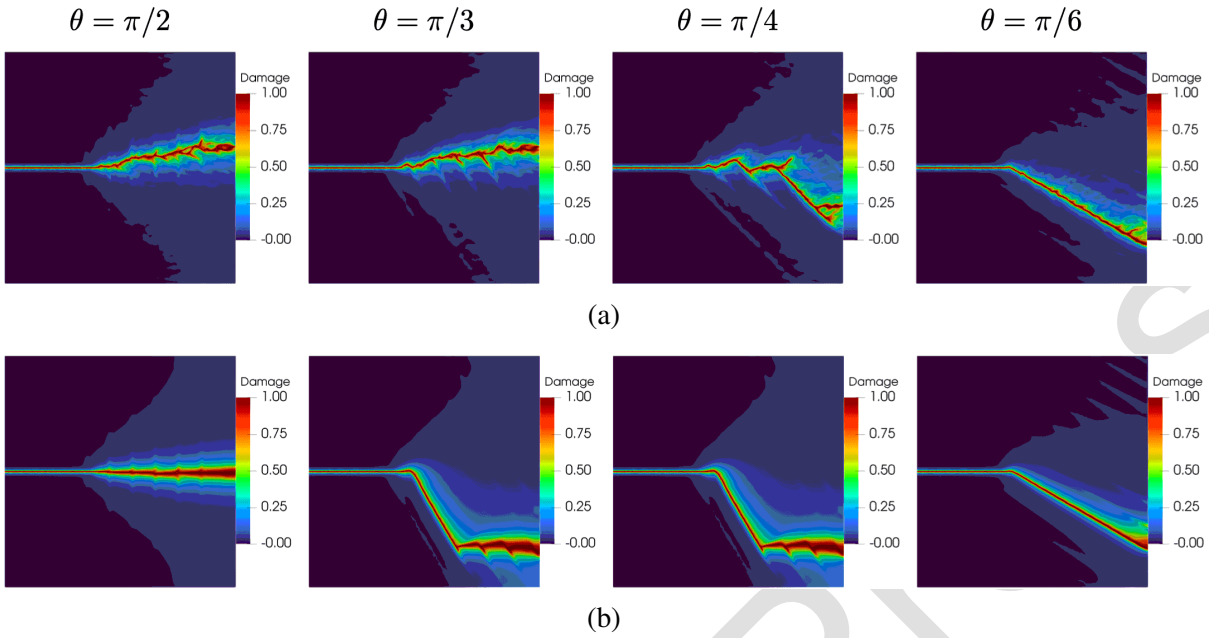

Fig. 7. Crack propagation snapshots for different angles θ: $\pi/2$, $\pi/3$, $\pi/4$, and $\pi/6$ (from left to right) in (a) heterogeneous and (b) homogeneous materials at final time $t = 50$. The red and blue colors represent cracked and uncracked areas, respectively, while the others indicate broken areas

property parameter becomes smaller and the maximum value becomes larger (see Table 2). This results in a very wide range of random physical property parameters, see Fig. 2. Consequently, at some points, the material will have small physical property values, while at other points, it will have large values. As a result, cracks will easily propagate through areas with small

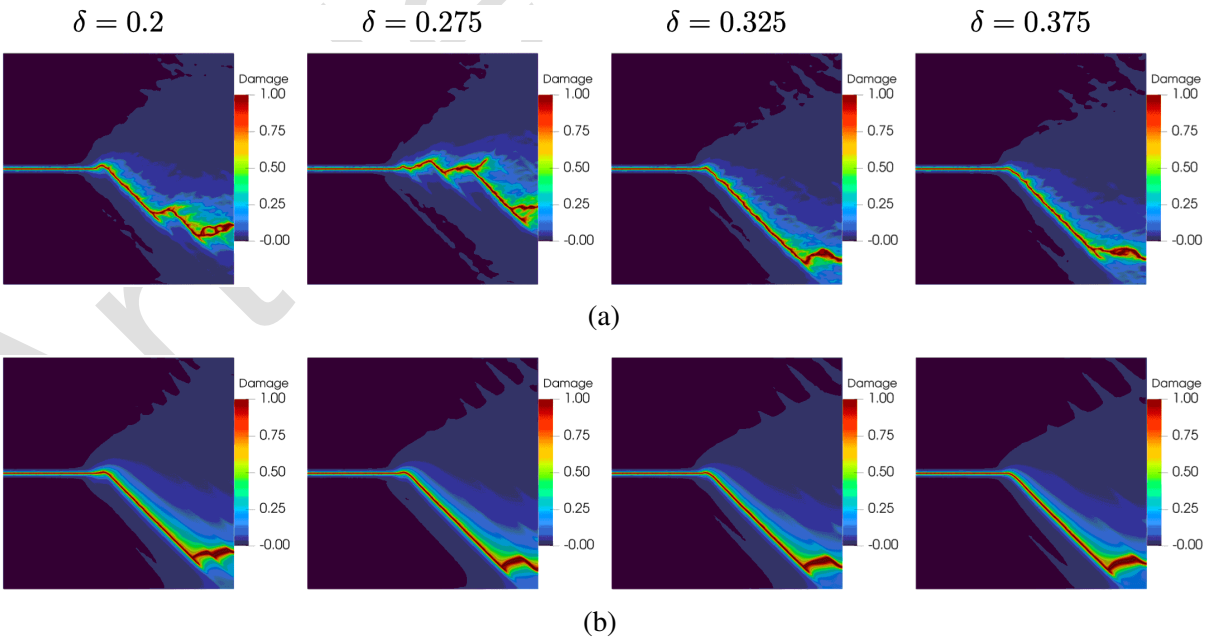

Fig. 8. Crack propagation snapshots for different widths δ: 0.2, 0.275, 0.325, and 0.375 (from left to right) in (a) heterogeneous and (b) homogeneous materials at final time $t = 50$. The red and blue colors represent cracked and uncracked areas, respectively, while the others indicate broken areas

Table 2. Maximum and minimum x_r for different m and $x_0 = 1.25$

Homogeneity index m	Random parameters x_r		
	Max	Min	Mean
1.25	9.029 93	0.000 194 3	1.159 6
2.00	4.301 74	0.005 207 8	1.104 91
3.00	2.849 26	0.032 364 9	1.114 28
7.00	1.779 35	0.261 118	1.168 44
10.0	1.600 5	0.417 695	1.188 58
40.0	1.329 68	0.950 38	1.232 56

physical property values. This is what happens at $m = 1.25, 2.0, 3.0, 7.0$. Branching cracks occur at several points because the physical properties are small at those points. However, the branch cracks do not grow larger because they encounter areas with large physical properties [18, 42, 45]. As a note, the value of m can be associated with specific rock materials based on experimental data. Different rock types exhibit varying values of this parameter due to differences in microstructure, grain size, porosity, and crack density [29].

Another implication of a small m value is that the material is easily damaged, as shown in Fig. 5. These results are consistent with previous studies that investigated the effect of the m value on material strength [28, 38, 44]. Meanwhile, in Example II, the influence of heterogeneity is also a strong reason why crack behavior in heterogeneous materials differs from that in homogeneous materials, even when considering the interface within the material. Especially for $\theta = \pi/6$ in the first case and $\delta = 0.325$ and 0.375 in the second case, the phenomenon of cracks being deflected and then growing along the interface occurs because it allows for generating low elastic energy (see Fig. 9) [8]. One of the major advantages of using the phase-field model for crack propagation studies is the automation of crack path selection based on minimizing the elastic energy, which is implicitly included in the phase-field model [23].

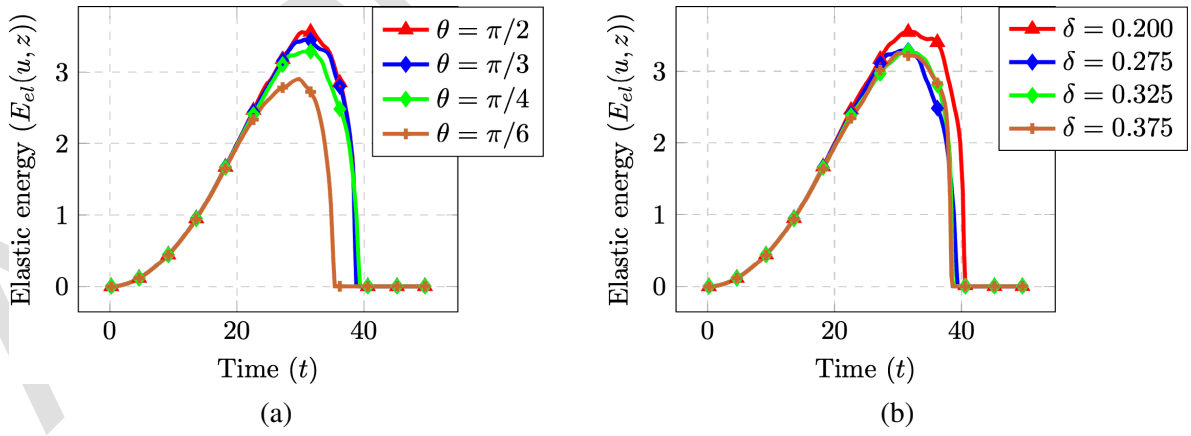

Fig. 9. Elastic energy profile for (a) different θ and (b) different δ during crack growth

4. Conclusions

The study of mode III crack propagation behavior, influenced by material heterogeneity using the phase-field model, has been conducted effectively. This research involved utilizing the

Weibull distribution function to generate heterogeneous materials. Meanwhile, the current study opts for the adaptive finite element method to solve the crack propagation equation.

1. The homogeneity index influences crack propagation behavior. In mode III cracks, materials with a small homogeneity index will produce a branched, tangled, and deflected crack propagation pattern, while materials with a large homogeneity index will produce straight cracks.
2. Material strength is influenced by the homogeneity index. The smaller the homogeneity index value, the weaker the material. Conversely, materials with a large homogeneity index value are stronger.
3. The effect of heterogeneity on crack propagation behavior in a material with an interface is insignificant at small angles and large distances between interfaces.

Although this research has effectively explained mode III crack propagation in heterogeneous materials, several interesting points remain regarding the future development and application of this research. The first key point is the setting of the small regularization parameter for length ε with respect to the Young's modulus, energy release rate, and tensile strength [31]. In the present study, we did not consider these parameters for simplicity. Therefore, we plan to address them in future research.

The second point is the application of the Weibull distribution function to generate heterogeneous physical properties in rock-like materials and porous media. This approach will be of interest for studying crack propagation due to mixed modes, hydraulic fracturing, and desiccation cracking in rock-like materials and porous media. We will address these issues in our future research by combining them with the Weibull distribution function.

Acknowledgements

The present work was partially supported by the Directorate of Research, Technology, and Community Service (DRTPM) of the Ministry of Education, Culture, Research, and Technology, through the Fundamental Research Scheme under grant numbers 049/E5/PG.02.00.PL/2024 and 05/UN29.20/PG/2024.

References

[1] Abdoh, D. A., Yin, B. B., Kodur, V. K. R., Liew, K. M., Computationally efficient and effective peridynamic model for cracks and fractures in homogeneous and heterogeneous materials, Computer Methods in Applied Mechanics and Engineering 399 (2022) No. 115318. https://doi.org/10.1016/j.cma.2022.115318

[2] Aldakheel, F., Noii, N., Wick, T., Wriggers, P., A global-local approach for hydraulic phase-field fracture in poroelastic media, Computers & Mathematics with Applications 91 (2021) 99–121. https://doi.org/10.1016/j.camwa.2020.07.013

[3] Alfat, S., Phase field model for crack propagation and its extension to thermoelasticity and poroelasticity: Thermal fracturing, hydraulic fracturing, and desiccation cracking, Ph.D. thesis, Kanazawa University, Kanazawa, 2023.

[4] Alfat, S., On energy-consistency principle of PFM for thermal fracturing in thermoviscoelasticity solids and its application for modeling thermal response due to crack growth based on adaptive mesh technique, Computers & Mathematics with Applications 175 (2024) 107–118. https://doi.org/10.1016/j.camwa.2024.09.016

[5] Alfat, S., New frameworks of PFM for thermal fracturing in the linear thermoelasticity solids based on a microforce balance approach, Physica D: Nonlinear Phenomena (2025) No. 134498. https://doi.org/10.1016/j.physd.2024.134498

[6] Alfat, S., Kimura, M., A micromechanical simulation of crack propagation in heterogeneous composite solid, Proceedings of the JSIAM Annual Meeting 2019, volume 3, 2019, pp. 3–4.

[7] Alfat, S., Kimura, M., Maulana, A. M., Phase field models for thermal fracturing and their variational structures, Materials 15 (7) (2022) No. 2571. https://doi.org/10.3390/ma15072571

[8] Alifian, M. M., Kimura, M., Alfat, S., Numerical crack path selection problem based on energy profiles, Japan Journal of Industrial and Applied Mathematics 39 (3) (2022) 817–841. https://doi.org/10.1007/s13160-022-00523-0

[9] Ambati, M., Gerasimov, T., De Lorenzis, L., Phase-field modeling of ductile fracture, Computational Mechanics 55 (2015) 1 017–1 040. https://doi.org/10.1007/s00466-015-1151-4

[10] Ambrosio, L., Tortorelli, V. M., On the approximation of free discontinuity problems, Bollettino dell'Unione Matematica Italiana 6 (1992) 105–123.

[11] Borden, M. J., Isogeometric analysis of phase-field models for dynamic brittle and ductile fracture, Ph.D. thesis, University of Texas at Austin, Austin, 2012.

[12] Borden, M. J., Verhoosel, C. V., Scott, M. A., Hughes, T. J. R., Landis, C. M., A phase-field description of dynamic brittle fracture, Computer Methods in Applied Mechanics and Engineering 217–220 (2012) 77–95. https://doi.org/10.1016/j.cma.2012.01.008

[13] Bourdin, B., Francfort, G. A., Marigo, J.-J., Numerical experiments in revisited brittle fracture, Journal of the Mechanics and Physics of Solids 48 (4) (2000) 797–826. https://doi.org/10.1016/S0022-5096(99)00028-9

[14] Chen, W., Konietzky, H., Liu, C., Tan, X., Hydraulic fracturing simulation for heterogeneous granite by discrete element method, Computers and Geotechnics 95 (2018) 1–15. https://doi.org/10.1016/j.compgeo.2017.11.016

[15] Cui, C., Ma, R., Martínez-Pañeda, E., A generalised, multi-phase-field theory for dissolution-driven stress corrosion cracking and hydrogen embrittlement, Journal of the Mechanics and Physics of Solids 166 (2022) No. 104951. https://doi.org/10.1016/j.jmps.2022.104951

[16] Eckardt, S., Könke, C., Adaptive damage simulation of concrete using heterogeneous multiscale models, Journal of Algorithms & Computational Technology 2 (2) (2008) 275–298. https://doi.org/10.1260/174830108784646661

[17] Ferro, N., Micheletti, S., Perotto, S., Anisotropic mesh adaptation for crack propagation induced by a thermal shock in 2D, Computer Methods in Applied Mechanics and Engineering 331 (2018) 138–158. https://doi.org/10.1016/j.cma.2017.11.024

[18] Guo, J., Lu, Q., Chen, H., Wang, Z., Tang, X., Chen, L., Quantitative phase field modeling of hydraulic fracture branching in heterogeneous formation under anisotropic in-situ stress, Journal of Natural Gas Science and Engineering 56 (2018) 455–471. https://doi.org/10.1016/j.jngse.2018.06.009

[19] Gurtin, M. E., Generalized Ginzburg-Landau and Cahn-Hilliard equations based on a microforce balance, Physica D: Nonlinear Phenomena 92 (3–4) (1996) 178–192. https://doi.org/10.1016/0167-2789(95)00173-5

[20] Hecht, F., New development in freefem++, Journal of Numerical Mathematics 20 (3–4) (2012) 251–266. https://doi.org/10.1515/jnum-2012-0013

[21] Heider, Y., Sun, W.-C., A phase field framework for capillary-induced fracture in unsaturated porous media: Drying-induced vs. hydraulic cracking, Computer Methods in Applied Mechanics

and Engineering 359 (2020) No. 112647. https://doi.org/10.1016/j.cma.2019.112647

[22] Karma, A., Kessler, D. A., Levine, H., Phase-field model of mode III dynamic fracture, Physical Review Letters 87 (2001) No. 045501. https://doi.org/10.1103/PhysRevLett.87.045501

[23] Kimura, M., Takaishi, T., Alfat, S., Nakano, T., Tanaka, Y., Irreversible phase field models for crack growth in industrial applications: Thermal stress, viscoelasticity, hydrogen embrittlement, SN Applied Sciences 3 (9) (2021) No. 781. https://doi.org/10.1007/s42452-021-04593-6

[24] Kimura, M., Takaishi, T., Tanaka, Y., What is the physical origin of the gradient flow structure of variational fracture models?, Philosophical Transactions A 382 (2277) (2024) No. 20230297. http://doi.org/10.1098/rsta.2023.0297

[25] Kuhn, C., Numerical and analytical investigation of a phase field model for fracture, Ph.D. thesis, Technische Universität Kaiserslautern, Kaiserslautern, 2013.

[26] Leclerc, W., Haddad, H., Guessasma, M., On the suitability of a discrete element method to simulate cracks initiation and propagation in heterogeneous media, International Journal of Solids and Structures 108 (2017) 98–114. https://doi.org/10.1016/j.ijsolstr.2016.11.015

[27] Levy, M., Vicentini, F., Yosibash, Z., Crack nucleation in heterogeneous bars: h-and p-FEM of a phase field model, Computational Mechanics 74 (3) (2024) 661–681. https://doi.org/10.1007/s00466-024-02449-5

[28] Li, H., Yang, C., Ding, X., William, N. T., Yin, H., Zhang, S., Weibull linear parallel bond model (WLPBM) for simulating micro-mechanical characteristics of heterogeneous rocks, Engineering Analysis with Boundary Elements 108 (2019) 82–94. https://doi.org/10.1016/j.enganabound.2019.07.018

[29] Liu, H. Y., Roquete, M., Kou, S. Q., Lindqvist, P.-A., Characterization of rock heterogeneity and numerical verification, Engineering Geology 72 (1–2) (2004) 89–119. https://doi.org/10.1016/j.enggeo.2003.06.004

[30] Luo, C., Sanavia, L., De Lorenzis, L., Phase-field modeling of drying-induced cracks: Choice of coupling and study of homogeneous and localized damage, Computer Methods in Applied Mechanics and Engineering 410 (2023) No. 115962. https://doi.org/10.1016/j.cma.2023.115962

[31] Mandal, T. K., Phase field fracture modelling of solids: Dynamics, anisotropy, and multi-physics, Ph.D. thesis, Monash University, Melbourne, 2021.

[32] Pillai, U., Heider, Y., Markert, B., A diffusive dynamic brittle fracture model for heterogeneous solids and porous materials with implementation using a user-element subroutine, Computational Materials Science 153 (2018) 36–47. https://doi.org/10.1016/j.commatsci.2018.06.024

[33] Qin, M., Yang, D., Chen, W., Numerical investigation of hydraulic fracturing in a heterogeneous rock mass based on peridynamics, Rock Mechanics and Rock Engineering 56 (6) (2023) 4 485–4 505. https://doi.org/10.1007/s00603-023-03299-y

[34] Sarmadi, N., Harrison, M., Mousavi Nezhad, M., Fisher, Q. J., Hydraulic fracture propagation in layered heterogeneous rocks with spatially non-Gaussian random hydromechanical features, Rock Mechanics and Rock Engineering 57 (2024) 8 117–8 140. https://doi.org/10.1007/s00603-024-03954-y

[35] Sparrow, E. M., Chukaev, A., Forced-convection heat transfer in a duct having spanwise-periodic rectangular protuberances, Numerical Heat Transfer 3 (2) (1980) 149–167. https://doi.org/10.1080/01495728008961752

[36] Su, Y., Zhu, J., Long, X., Zhao, L., Chen, C., Liu, C., Statistical effects of pore features on mechanical properties and fracture behaviors of heterogeneous random porous materials by phase-field modeling, International Journal of Solids and Structures 264 (2023) No. 112098.

https://doi.org/10.1016/j.ijsolstr.2022.112098

[37] Takaishi, T., Kimura, M., Phase field model for mode III crack growth in two dimensional elasticity, Kybernetika 45 (4) (2009) 605–614.

[38] Tang, C. A., Liu, H., Lee, P. K. K., Tsui, Y., Tham, L. G., Numerical studies of the influence of microstructure on rock failure in uniaxial compression – Part I: Effect of heterogeneity, International Journal of Rock Mechanics and Mining Sciences 37 (4) (2000) 555–569. https://doi.org/10.1016/S1365-1609(99)00121-5

[39] Vicentini, F., Carrara, P., De Lorenzis, L., Phase-field modeling of brittle fracture in heterogeneous bars, European Journal of Mechanics-A/Solids 97 (2023) No. 104826. https://doi.org/10.1016/j.euromechsol.2022.104826

[40] Wang, M., Yu, Z., Jin, Y., Shao, J., Modeling of damage and cracking in heterogeneous rock-like materials by phase-field method, Mechanics Research Communications 114 (2021) No. 103612. https://doi.org/10.1016/j.mechrescom.2020.103612

[41] Wong, T.-F., Wong, R. H. C., Chau, K. T., Tang, C. A., Microcrack statistics, Weibull distribution and micromechanical modeling of compressive failure in rock, Mechanics of Materials 38 (7) (2006) 664–681. https://doi.org/10.1016/j.mechmat.2005.12.002

[42] Worthington, M., Chew, H., Crack path predictions in heterogeneous media by machine learning, Journal of the Mechanics and Physics of Solids 172 (2023) No. 105188. https://doi.org/10.1016/j.jmps.2022.105188

[43] Xu, B., Xu, T., Xue, Y., Heap, M. J., Wasantha, P. L. P., Li, Z., Phase field modeling of mixed-mode crack in rocks incorporating heterogeneity and frictional damage, Engineering Fracture Mechanics 298 (2024) No. 109936. https://doi.org/10.1016/j.engfracmech.2024.109936

[44] Xu, Y., Yao, W., Xia, K., Numerical study on tensile failures of heterogeneous rocks, Journal of Rock Mechanics and Geotechnical Engineering 12 (1) (2020) 50–58. https://doi.org/10.1016/j.jrmge.2019.10.002

[45] Yang, Y. F., Li, G., Liang, Z. Z., Tang, C. A., Numerical investigation on crack branching during collision for rock-like material, Theoretical and Applied Fracture Mechanics 76 (2015) 35–49. https://doi.org/10.1016/j.tafmec.2014.12.010

Appendix

In this section, we demonstrate the energy dissipation equality of the phase-field model for crack propagation using the Clausius-Duhem inequality. We consider the second law of thermodynamics, represented by the Clausius-Duhem inequality, for the original phase-field model for crack propagation as described in [5]

$$D^* = \sigma_z[u] : e[\dot{u}] + B^* \dot{z} + H^* \cdot \nabla \dot{z} - \dot{\Psi}^* \geq 0. \tag{16}$$

Here, $\sigma_z = (1-z)^2\, C\, e[u]$ represents the modified stress tensor, $e[\dot{u}]$ denotes the partial derivative of the strain tensor $e[u]$ with respect to time, while the term

$$\dot{\Psi}^* = \frac{d}{dt}\left[\frac{1}{2}\sigma_z[u] : e[u] + \frac{1}{2}\gamma\left(\varepsilon|\nabla z|^2 + \frac{|z|^2}{\varepsilon}\right)\right]$$

is the Helmholtz free energy of the original phase-field model for crack propagation. Since we are applying crack propagation in anti-plane displacement, the Clausius-Duhem inequality

in (16) becomes

$$D^* = (1-z)^2\mu\nabla u\cdot\nabla\dot{u} + B^*\dot{z} + H^*\cdot\nabla\dot{z} - \frac{d}{dt}\left[\frac{1}{2}(1-z)^2\mu|\nabla u|^2 - \frac{1}{2}\gamma\left(\varepsilon|\nabla z|^2 + \frac{|z|^2}{\varepsilon}\right)\right] \geq 0. \tag{17}$$

Since (9)–(10) are substituted into (17), we obtain the following energy dissipation:

$$D^* = \alpha|\dot{z}|^2 \geq 0. \tag{18}$$

This result is consistent with (7).